X-, KA-, AND W-BAND RADAR OBSERVATIONS OF PRECIPITATING CLOUDS IN THE ARCTIC

Mariko Oue*, Johannes Verlinde, and Eugene E. Clothiaux
The Pennsylvania State University, University Park, Pennsylvania

1. INTRODUCTION

Short-wavelength radars (e.g., W-, Ka, and X-bands) are valuable instruments for investigations of ice hydrometeors. Many studies simulated backscattering for snow particles and showed inconsistencies of backscattering cross sections between the short wavelength radars (e.g., Botta et al., 2011; Botta et al., 2013). In Recent years, several studies approached to retrieve microphysical characteristics taking advantage of dual frequency ratio (DFR) of reflectivities among multiple frequency radars. Kneifel et al. (2011) pointed out that concurrent use of Ku/Ka band and Ka/W band DFRs allows for a separation of different snow particle habits. Leinonen et al. (2012) exhibited characteristics of DWR of snow aggregates by collocated Ku-, Ka-, and W-band radar measurements. These studies focused on pure ice clouds and avoided complexities the DFR from attenuation by liquid water.

In the Arctic, mixed-phase clouds, which are composed of supercooled liquid drops and ice crystals, are commonly observed (Curry et al., 1996; Intrieri et al., 2002). The mixed-phase clouds persist in the boundary layer from a few days to a couple of weeks. For understanding microphysics in the Arctic, clarification of characteristics of short-wavelength radar parameters in the mixed-phase clouds and pure ice clouds is an important subject.

To observe the Arctic clouds, Ka-, W-, and X-band polarimetric radars have been installed by the Department of Energy (DOE) Atmospheric Radiation Measurements (ARM) program in Barrow, Alaska. However, characteristics of radar reflectivity (Z_h) and polarimetric parameters (e.g., linear depolarization ratio, LDR; differential reflectivity, ZDR) in the Arctic are unclear. The purpose of this study is to demonstrate characteristics of reflectivity from the Ka-, W-, and X-band polarimetric radars in the Arctic clouds from the preliminary analysis. In particular, we investigate features of Z_h and LDR values from the Ka-, W-, and X-band polarimetric radars in Arctic mixed-phase clouds and ice clouds with low liquid water.

* *Corresponding author address:* Mariko Oue, Pennsylvania State Univ., Dept. of Meteorology, Pennsylvania, PA 16802; e-mail: muo15@psu.edu.

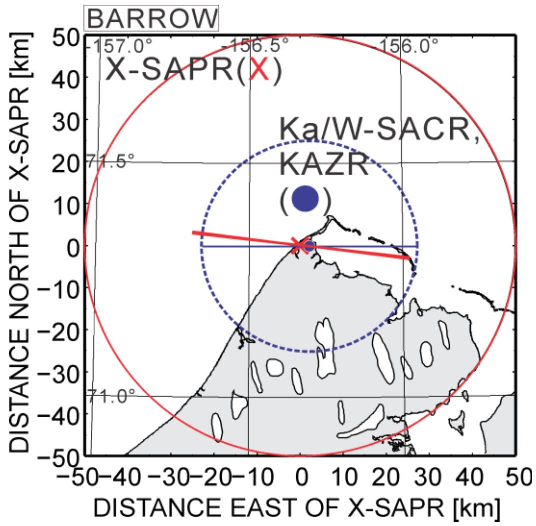

Fig. 1 Locations of the Ka- and W-SACRs (solid circle) and the X-SAPR (cross mark) and observation ranges of the Ka- and W-SACR radars (large circle by dashed line) and the X-SAPR radar (large circle by solid line). Blue and red lines represent RHI directions of the Ka- and W-SACR radars and the X-SAPR radars, respectively.

2. DATA

This study uses the Ka- and W-band scanning ARM cloud radars (Ka-SACR and W-SACR, respectively), the X-band scanning ARM precipitation radar (X-SAPR), and Ka-band zenith ARM radar (KAZR) located in by the DOE ARM program Climate Research Facility (ACRF) at North Slope of Alaska (NSA) in Barrow (Fig. 1). The Ka- and W-SACR radars are collocated and perform RHI scans toward same directions simultaneously. While, the X-SAPR is located at approximately 2 km to the west of the W- and Ka-SACR radars and performed RHI scans independently from the Ka- and W-SACR radars. In addition to the RHI scans, the three scanning radars collected vertically pointing data. Meanwhile, the KAZR radar is collocated with the Ka- and W-SACR radars and collected vertically pointing data at all times. Specifications and observation settings of these radars are listed in Table 1.

The Z_h from the three scanning radars (Ka- and W-SACR and X-SAPR radars) have unknown offsets respectively. Therefore, this study performs

Table 1. Specifications and configurations of radars.

	W-SACR (Scanning)	Ka-SACR (Scanning)	KAZR (Vertically pointing)	X-SAPR (Scanning)
Frequency	93.93 GHz	35.29 GHz	34.89 GHz	9.67 GHz
Polarization	H transmit and simultaneous H&V receive			Simultaneous H&V transmit and receive
Beam width	0.33°	0.33°	0.3°	1.0°
Pulse repetition frequency	4950 Hz	4960 Hz	2771.31 Hz	1950 Hz
Pulse width	333 µs	1333 µs	4.0 µs (long pulse)	0.5 µs
Range spacing	25 m	25 m	30 m	75 m
Number of integration pulses	3	3	20	32 (80 since 6 Dec. 2012)
Observation range	25 km	25 km	17.5 km	50 km

inter comparisons using the KAZR Z_h and presents qualitative features in reflectivity fields.

A presence of liquid water in clouds is confirmed by a high spectral resolution lidar and a microwave radiometer located in the ACRF at NSA.

To compare high-liquid clouds with low-liquid clouds, this study show a mixed-phase cloud case on 17 October, 2012 (high-liquid clouds) and a snow case accompanying little liquid water on 13 January, 2013 (low-liquid clouds). In both cases, temperatures were below 0°C in all layers, and precipitation particles consisted of ice. In both cases, datasets of concurrent RHI scans from the W- and Ka-SACR and the X-SAPR radars are available. However, vertically pointing data of the X-SAPR radar on 17 October was not available.

3. RESULTS

3.1 *Comparisons of Z_h in vertically pointing*

In order to investigate offsets in Z_h, the Z_h values from three scanning radars are compared with Ka-band Z_hs from the KAZR radar using vertically pointing data. Figure 2 shows comparisons of Z_h from the Ka-, W-, and X-band scanning radars with the Ka-band Z_h from the KAZR radar for high-liquid and low-liquid cloud cases. To compare these radar data, data from each radar are averaged with a resolution of 150 m in range since the spatial resolutions are different among these radars.

Compared with the KAZR radar, the Ka-SACR Z_h has a constant offset of approximately -6.5 dB. Meanwhile, the X-band Z_h has a constant offset with $-15 \leq Z_h < 15$ dBZ and shift to larger values with $Z_h > 15$ dBZ. The shift toward larger values in the X-band Z_h with $Z_h > 15$ dBZ (i.e., shift toward smaller values in Ka-band Z_h) is probably derived from the Mie scattering effects with large snow particles. With low Z_h values less than -15 dBZ, the X-band Z_hs seem to reach the noise level. On the other hand, the W-band Z_h has variable offsets between the two cloud cases. Especially, the W-band Z_h values drastically shift toward smaller Z_h with the Ka-band $Z_h \geq 5$ dBZ.

3.2 *High-liquid clouds*

To reveal causes of the negative shift in the W-band Z_h and the positive shift in the X-band Z_h with respect to the Ka-band Z_h for the high-liquid cloud case on 17 October, 2012, Z_hs and LDR in RHIs are analyzed. On that day, the high spectral resolution lider measured distinct liquid cloud signals in several layers below a height of 1.7 km.

Figure 3 shows a vertical cross section of Ka-band Z_h observed by a Ka-SACR RHI scan and received power from the Ka- and W-SACR radars at 1634 UTC on 17 October 2012. The Z_h values reach up to 15 dBZ below a height of 2 km. Compared with the Ka-band received power, the W-band received powers quickly drop to the noise level around a range of 20 km. The significant decreases of the power are shown below a height of 1.5 km, where liquid cloud layers were present. The significant attenuation was probably derived by the liquid clouds.

To investigate the positive shift in the X-band Z_h, the Z_h values from the X-SAPR and Ka-SACR radars are compared. Figure 4 shows paths of Z_h and LDR at elevation angles of 4° and 15°. These paths were averaged with 1° elevation and 150 m range resolutions. The Z_h values were calibrated by offsets estimated by comparisons with the KAZR Z_h. The X-band Z_hs at 4° are larger than the Ka-band Z_h. At the elevation angle of 15°, the X-band Z_h values are larger than the Ka-band Z_h up to 6 km in range, and are consistent with the Ka-band Z_h beyond the range of 6 km. This suggests little attenuation in Ka-band Z_h. The region of larger X-band Z_hs are found below a height of 2 km.

In the regions of larger X-band Z_h, the LDR values measured by the Ka-SACR radar are 5-10 dB larger than the minimum LDR. The larger LDR values indicate a presence of large dendrites, rimed dendrites, or aggregates. These ice particles

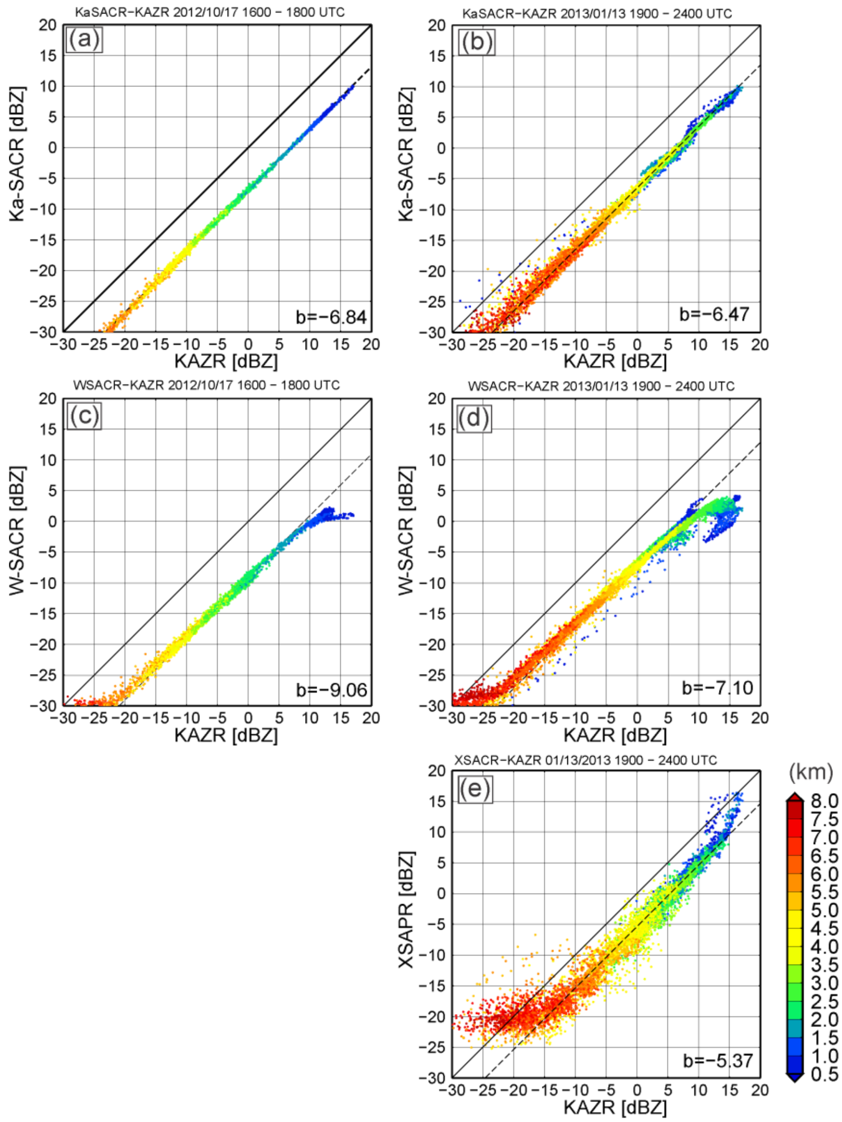

Fig. 2. Scattering Z_h diagrams of (a)(b) the KAZR radar versus the Ka-SACR radar , (c)(d) the KAZR radar versus the W-SACR radar, and (e) the KAZR radar versus the X-SAPR radar for (a)(c) 17 October, 2012 and (b)(d)(e) 13 January, 2013. Data were collected by vertical pointing observations and averaged averaged with a resolution of 150 m in range. Color scale represents height. The intercept parameter of fitted line (dashed line) is shown on the bottom on each panel.

could derive resonance effects in Ka- and W-band radars. Furthermore, sufficiently-large particles compared to the radar wavelength derive the Mie scattering effects. The positive shift in the X-band Z_h would be derived from resonance and Mie scattering effects with large ice particles.

3.2 ***Low-liquid clouds***

To reveal causes of the DFRs for the low-liquid cloud case on 13 January, 2013. On that day, the high spectral resolution lider measurement showed no noticeable liquid signal. A microwave radiometer retrieved little amount of liquid water path (~5 g m^{-2}).

A vertical cross section of Z_h observed by the Ka-SACR RHI scan at 1958 UTC on 13 January 2013 and elevation dependencies of normalized DFR of the Ka-band Z_h to the W-band Z_h (Ka/W) are displayed in Fig 5. In the RHI, Z_h values reach up to 12 dBZ (Fig 5a). The Z_h values are included in a region of constant offset in X-band Zh shown in Fig. 2e ($-15 \le Z_h < 15$ dBZ). The normalized DFRs were estimated by DFRs of Ka/W divided by the DFR value with an elevation angle of 90°. In the elevation dependencies, the normalized DFR values at heights of 0.2-0.8 km and 1.0-1.5 km were averaged every

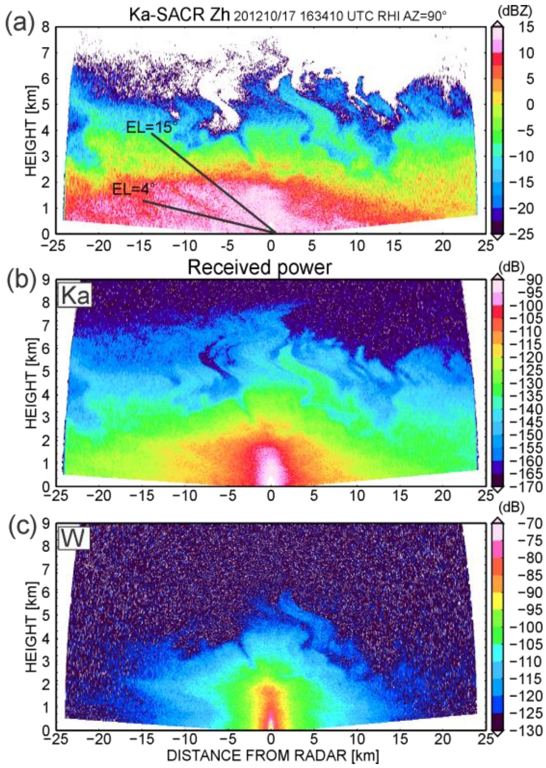

Fig. 3. Vertical cross sections of (a) the Ka-SACR Z_h, (b) the Ka-SACR received power, and (c) the W-SACR received power from the RHI scan at an azimuth angle of 90° at 1634 UTC on 17 October 2012. Solid lines in (a) represent elevation angles of 4° and 15° used in Fig. 4.

5° in elevation angle. The DFR of Ka/W shows large values around lower elevation angles. The DFR values decrease with increasing elevation angle. Since there was little liquid water in the clouds, it is likely that there were little effects of attenuation. Rather, the DFR of Ka/W is likely to be derived from resonance effects. The elevation dependency of resonance effects is consistent with scattering simulations presented by Botta et al. (2013).

Comparisons of X-band Z_h with Ka-band Z_h are shown in Fig. 6. Figure 6 shows paths of Z_h at elevation angles of 4° and 15°. The X-band Z_hs are mostly consistent with the Ka-band Z_hs with both elevation angles, but the X-band Z_h values in lower altitudes below a height of 0.6 km at 4° are slightly larger. The larger X-band Z_h at the low elevation angle would be derived from resonance effects, as well as the DFR of Ka/W in the low-liquid clouds.

4. SUMMARY

Ice precipitating clouds with high-liquid water clouds and those with low-liquid water were observed by the W-, Ka-, and X-band polarimetric radars.

The W-band Z_h was strongly attenuated in the high-liquid clouds. The DFR of Ka/W would result from attenuation by liquid water significantly, not only resonance and Mie scattering effects with ice particles. Meanwhile, the X-band Z_hs were larger than the Ka-band Z_hs corresponding to large Z_h (≥15 dBZ) and large LDRs. The large LDR values indicated a presence of snow particles of dendrites, rimed dendrites and aggregates. The positive shift in the X-band Z_h would be derived from resonance and Mie scattering effects with large ice particles.

In the low-liquid clouds, the DFR of Ka/W showed larger values at lower elevation angles and large elevation dependencies. Meanwhile, the X-band Z_hs

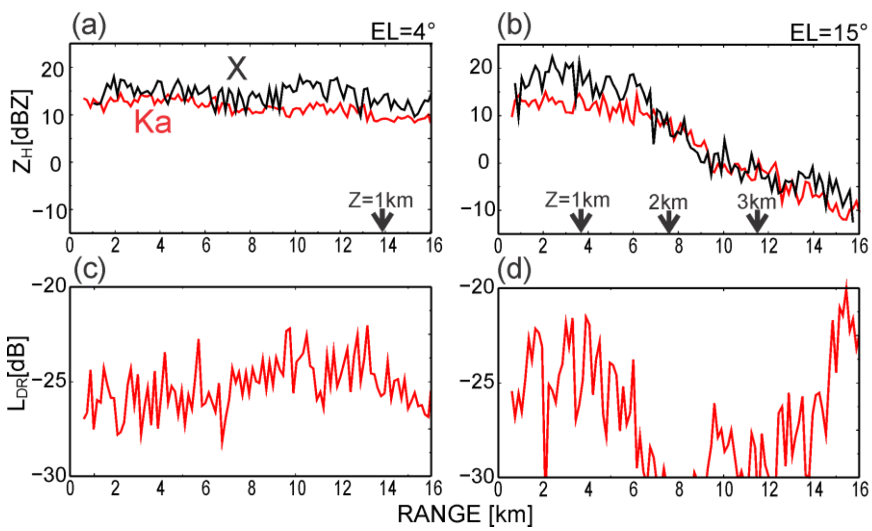

Fig. 4. Paths of (a)(b) Z_hs from the X-SAPR (black lines) and Ka-SACR (red lines) radars and (c)(d) LDRs from the Ka-SACR radar at elevation angles of (a)(c) 4° and (b)(d) 15° in RHI scans at 1634 UTC for the Ka-SACR radar and 1635 UTC for the X-SAPR radar on 17 October. These paths were averaged with 1° elevation and 150 m range resolutions. Arrows on the bottom on (a) and (b) indicate heights.

were slightly larger in lower altitudes. These DFRs of Ka/W and X/Ka would be mostly derived from resonance effects with the ice crystals.

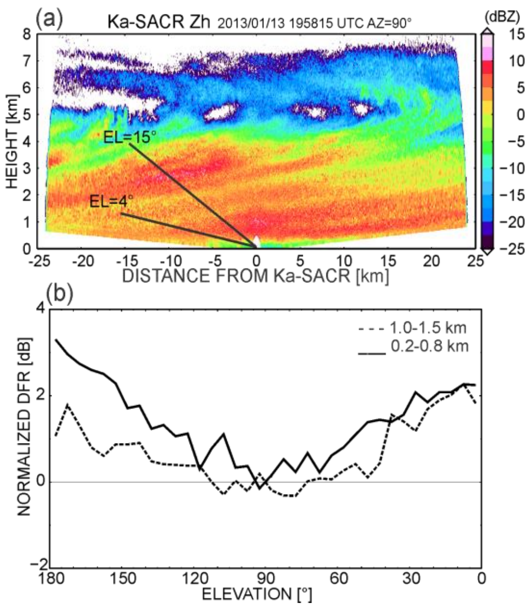

Fig. 5. Vertical cross sections of (a) the Ka-SACR Z_h, (b) elevation dependencies of normalized DFRs of Ka-SACR radar to the W-SACR radar from the RHI scan at an azimuth angle of 90° at 1958 UTC on 13 January 2013. The normalized DFRs were estimated by DFRs of Ka/W divided by the DFR value at an elevation angle of 90°. The normalized DFR values at heights of 0.2-0.8 km (solid line) and 1.0-1.5 km (dashed line) were averaged every 5° in elevation angle. Solid lines in (a) represent elevation angles of 4° and 15°used in Fig. 6.

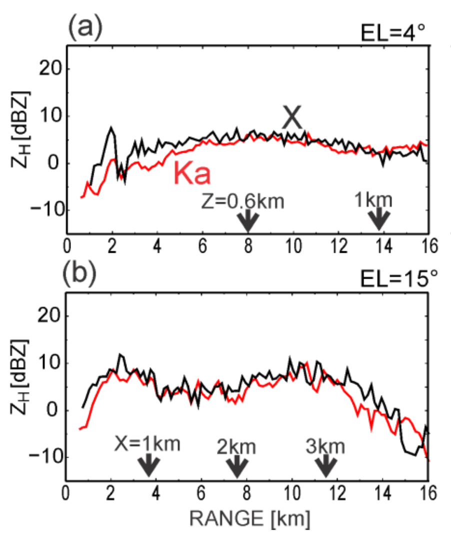

Fig. 6. Same as Figs. 4a and 4b, but for 1958 UTC for the Ka-band and 2000 UTC for the X-band on 13 January, 2013.

ACKNOWLEDGMENTS

This study was funded by the Department of Energy Atmospheric System Research Grant DE-FG02-05ER64058 and partly supported by the Office of Postdoctoral Affairs of the Pennsylvania State University.

REFERENCES

Botta, G., K. Aydin, and J. Verlinde, 2013: Variability in millimeter wave scattering properties of dendric ice crystals. *J. Quantitative Spectroscopy and Radiative Transfer*, in press.

Botta, G., K. Aydin, and J. Verlinde, A. E. Avramov, A. S. Ackerman, A. M. Fridlind, G. M. McFarquhar, and M. Wolde, 2011: Milimeter wave scattering from ice crystals and their aggregates: Comparing cloud model simulations with X- and Ka band radar measurements. *J. Geophys. Res.*, 116, D00T04. doi:10.1029/2011JD015909.

Curry, J. A., W. B. Rossow, D. Randall, and J. L. Schramm, 1996: Overview of Arctic clouds and radiation characteristics. *J. Clim.*, **9**, 1731–1764.

Intrieri, J. M., M. D. Shupe, T. Uttal, and B. J. McCarty, 2002: An annual cycle of Arctic cloud characteristics observed by radar and lidar are SHEBA. *J. Geophys. Res*., 107(C10), 8030, doi:10.1029/2000JC000423.

Kneifel, S., M. S. Kulie, and R. Bennartz, 2011: A triple-frequency approach to retrieve microphysical snowfall parameters. *J. Geophys. Res.*, 116, D11203. doi:10.1029/2010JD015430.

Leinonen, J., S. Kneifel, D. Moisseev, J. Tyynela, S. Tanelli, and T. Nousiainen, 2012: Evidence of nonspheroidal behavior in millimeter-wavelength radar observations of snowfall. *J. Geophys. Res.*, 117, D18205, doi:10.1029/2010JD017680.